Revised 3

Determination of the Melting temperature of Kaolinite by means of the Z-method

Brahim K. Benazzouz,[1] Ali Zaoui,[1,*] and Anatoly B. Belonoshko[2]

[1]LGCgE-(EA 4515) Lille Nord de France, Polytech'Lille. Université des Sciences et de la Technologie de Lille. Cité Scientifique. Avenue Paul Langevin. 59655 Villeneuve D'Ascq Cedex, France

[2]Condensed Matter Theory, Department of Theoretical Physics, AlbaNova University Center, Royal Institute of Technology (KTH), 106 91 Stockholm, Sweden

Abstract

The melting temperature of materials is one of the more important thermodynamic properties. Despite the importance of Kaolinite, one of the most common clay minerals on the Earth's surface, its thermal behavior is only poorly understood.

We apply here the Z-method to determine the melting temperature (T_m) and the limit of superheating (T_{LS}) of kaolinite. The T_m is found at 1818 K (8.85 GPa), and T_{LS} at 1971 K (6.8 GPa). The diffusion coefficient for all atoms has been calculated in a broad temperature range. The calculated characteristics and, in particular, their dependence on temperature have confirmed the solid-liquid transition and strongly support the calculated melting point. In addition, some computed quantities, such as the radial distribution function, coordination numbers and mean-square displacement, were used to confirm the liquid state of kaolinite from the melting temperature as well as at other temperatures in the liquid branch. The diffusion coefficient for different atoms has been calculated throughout the isochore. These quantities and in particular their evolution under temperature have confirmed the solid-liquid states of kaolinite and the presence of the melting point. The latter quantity constitutes the first ever melting simulation of a clay with close agreement to the experimental one.

Keywords: Kaolinite, melting, molecular dynamics, Z-method

Introduction

Kaolinite is one of the most common clay minerals found on the Earth's crust. It is widely used in several engineering applications and in different industrial sectors such as the ceramic industry, and the manufacturing of paper, potteries, paints, and cosmetics, as well as a sorbent for pollutants (Ciullo 1996, Murray 2000, 2007).

The kaolinite structure and its transformation during heating were studied some years ago (Murray 2007). However, information about this system is still sparse in spite its obvious importance and its large availability. In pure form, the melting point of kaolinite is 2123 K (Murray 2007). Determining the melting point of materials is of significant importance for several applications in geophysics, geology and industry.

Computer simulations of melting revealed that the limit of superheating (T_{LS}) is higher by about 20–30% than the melting temperature (T_m) (Belonoshko et al. 2006). The prediction of the pressure dependence of the melting temperature is very important for solid materials, especially for geologists. Molecular dynamics (MD) simulations are a well-established technique in mineralogy, especially for studying the effects of high pressure and elevated temperature on the properties of solids and theirs melts. Among the studies on the calculation of overheating and melting curves using molecular dynamics calculations are those of Matsui and Price (1991), Belonoskho (1994), Ahuja et al. (1998), and Chaplot et al. (1998).

In this paper, we present a study of both the melting temperature (T_m) and the limit of superheating (T_{LS}) of kaolinite by means of molecular dynamics simulations and the Z-method. The latter is characterized by the use of a single-phase (solid) (Belonoshko et al. 2006, 2007).

Methods;

The clay force field (CLAYFF) was used to simulate the structure of kaolinite. The CLAYFF is already proven to be highly effective in modeling the crystal structure ofm different hydroxides, oxyhydroxides, and clay phases (Cygan et al. 2004). The structural, dynamical, and energetic properties of cement materials (Kirkpatrick et al. 2005; Kalinichev et al. 2007), the swelling behavior of Na-Montmorillonite (Zheng et al. 2010; Zheng et al. 2011) and the vibrational spectrum of Hydrotalcite (Cygan et al. 2004) have been investigated with the CLAYFF force field. Several properties have been addressed such as structural and dynamical properties of hydrated mineral systems and their interfaces with aqueous solutions (Greathouse and Cygan 2005; Wang et al. 2005; Vasconcelos and Bunker 2007), the vibrational spectroscopy of brucite and frequencies for Montmorillonite clay (Braterman and Cygan 2006; Kalra et al. 2007), the investigation of the structural and vibrational properties of Talc and Pyrophyllite (Larentzos et al. 2007), and the thermomechanical properties of a Montmorillonite crystal with oligomer intercalates (Mazo et al. 2008a, b and c).

Molecular dynamics calculations at the thermodynamic equilibrium were performed using the Nosé-Hoover method (Hoover 1985) in the DL_POLY simulation package (Smith and Forester 1996). The ensembles used here are the NPT (the number of particles N, pressure P, and temperature T are fixed during the simulation) with barostat and thermostat relaxation times of 0.5 ps. In the second part of the calculation, NVE (the number of particles N, volume V, and energy E are fixed during the simulation) was used.

The equations of motion were integrated by using the Verlet leapfrog integration algorithm (Verlet 1967;Allen and Tildesley 1989) with a time step of 1fs (1×10^{-15} s) and 0.5fs to ensure the conservation of energy. The Ewald summation (Ewald 1921) with a tolerance of 1×10^{-5} is applied in our study since it is the most satisfactory method for treating Coulombic long-range interactions. For short-range interactions, either spherical or “minimum image” cutoff

criteria are commonly used (Allen and Tildesley 1987; Frenkel and Smit 1996). The cut-off radius is $r_c = L_{min}/2$, where L_{min} is the smallest box length (in our system $L_{min} = L_x = 2.0614$ nm). The cutoff used for van der Waals interactions is around 0.85 nm. The pressure was maintained constant by using a Melchionna modification of the Hoover algorithm (Melchionna et al. 1993**)** in which the equations of motion involve a Nosé-Hoover thermostat and a barostat.

The Z-method was already used for a wide variety of materials such as molybdenum at high pressure and temperature (Belonoshko et al. 2008),hydrogen (Davis et al. 2008), Fe (Belonoshko et al. 2009) and others (Davis et al. 2009; Davis et al. 2010; Belonoshko et al. 2010; Burakovsky et al. 2010).

The method is characterized by the use of a single-phase (solid). The name of this method was given because of the characteristic shape, Z-letter, of the curve isochoric.

Here, all simulations have been performed in the NVE ensemble. The system is initially in the solid state, with a volume that remains fixed throughout the isochoric curve. The isochore consists of three branches: the first is crystalline, which in turn consists of two parts: a solid one and a superheated solid one above the melting point that is in the liquid region of the phase diagram. This is followed by an intermediate branch with negative slope which represents a transition from crystalline state to liquid state. The final and third branch is in the liquid state.

At the beginning of the simulation, the allocation of the kinetic energy to atoms in a solid system in the NVE ensemble initiates melting if the temperature is slightly higher than its limit of superheating (T_{LS}), without any change in the dynamic process. We note here that before arriving at the T_{LS}, the structure remains solid because the system of interaction of atoms is equilibrating when the initial kinetic energy is low. This energy starts to increase with T, and the system enters the superheated solid state across the melting curve. With these

different temperatures, we get an almost straight line to the point of T_{LS} in the solid branch (the upper cap of the Z letter).

Once the isochore reaches T_{LS}, the temperature drops to T_m because the latent heat of melting is removed from the kinetic energy. This part is called the intermediate branch that starts with T_{LS} and ends with T_m. It is a discontinuity in the straight line. Finally, at temperatures above T_m, the system begins to be liquid and then it forms an almost straight line, which is the liquid branch (the lower cap of the letter Z). Therefore, the point at the end of the solid branch represents the temperature limit of superheating T_{LS}, and the first point at the beginning of the curve is the melting temperature T_m. More details on this method are given elsewhere (Belonoshko et al. 2006; Belonoshko et al. 2007).

The simulation box used in our calculations is $4 \times 2 \times 3$ unit cells in the **a**, **b**, and **c** dimensions (24 kaolinite unit cells), with a total of 816 atoms in the solid. The corresponding L_x, L_y, and L_z dimensions are 20.614, 17.881, and 22.739 Å. The periodic boundary conditions are applied to all three directions.

Melting and thermal instability are different phenomena. There are several methods to determine the true melting temperature of a substance, as coexistence phases (Morris et al. 1994; Landman et al. 1986), two-phase (Belonoshko 1994) or the Z-method (Belonoshko et al. 2006, 2007).

Each pressure-temperature point in isochoric curve was obtained in NVE ensemble after 800TS000 steps, equivalent to 400 ps. To solve the equations of movement we used a time step of 0.5 fs to ensure the conservation of energy.

Results and discussions

Kaolinite is a 1:1 layered aluminosilicate clay mineral with an uncharged dioctahedral phyllosilicate structure. The layers stack along the **c** axis, and they are composed of a repeating layer of an aluminum octahedral (O) sheet and a silicon tetrahedral (T) sheet with a basal distance for the elementary layer, which varies between 7.1 and 7.4 Å. Each layer is formed by a sheet of SiO_4 tetrahedra forming six-membered rings connected via shared oxygen atoms to a sheet of AlO_6 octahedra forming four-membered rings. The tetrahedral-octahedral layers are electrically neutral.

The kaolinite structure (Fig. 1) contains two types of hydroxyl groups. The first one is bound to the six-coordinated aluminum atoms and covers one of the two basal surfaces of the layer. These hydroxyls are therefore called outer (or interlayer) hydroxyl groups. The second type of OH groups is located within the sheets extending from the aluminum octahedra (so-called internal or inner hydroxyl groups).

In this work, the kaolinite unit-cell content used is initially based on crystallographic data of Bish (Bish 1993), a unit cell of triclinic symmetry (*C*1) with lattice parameters a = 5.153, b = 8.941, c = 7.390 Å, and angles: α = 91.926°, β = 105.046°, γ = 89.797°. The thickness (basal distance) of the unit layer is d = 7.1329 Å. The unit cell has the chemical composition $2[Si_2Al_2O_5(OH)_4]$, which corresponds to 34 atoms and its density is 2.6 g/cm^3.

The computed isochore for kaolinite structure is shown in Figure 2. The superheating limit temperature and the melting point are also shown in the figure. The superheated limit temperature is estimated at the highest point in the solid branch, while the melting point is estimated at the lowest point of the liquid branch. The superheated temperature limit T_{LS} is 1971 K and the melting point T_m is 1818 K corresponding to pressures of 6.8 GPa and 8.85 GPa, respectively. This is in reasonable agreement with the only experimental measurement at

1 bar (Murray 2007). We found that the limit of superheating is higher than the melting temperature by about 7.8%.

A snapshot of the structure of kaolinite, at two temperatures on the solid branch isochore, is displayed in Figure 3. These temperatures are at 1688 K, where the structure is solid, and at T_{LS}. The structures in the solid branch retain their initial crystalline structures. Figure 3 also shows the snapshot of the structure in the intermediate isochore branch. We may see that the structure begins to be unstable followed by a disorder; then it becomes liquid. At T_m, atoms show very large thermal vibrations and the structure finally becomes liquid.

Various quantities were computed such as the radial distribution function (RDF), coordination numbers and mean-square displacement at different temperatures to confirm the liquid structure. The radial distribution function, denoted as g (r_{ij}), for the various atom–atom pairs, is a measure and a good indicator to determine the correlation between atoms within a system. The g(r) was calculated for all atom pairs. Here the RDF of Al-Al, Si-Si, Al-O_H, and O_H-H and the corresponding coordination numbers n(r) are presented in Figure 4 with increasing temperature.

We present the case of temperatures 1688 K, T_{LS} = 1971 K, 1911 K, T_m = 1818 K, and 2261 K corresponding to the temperatures on the solid branch, the limit of superheating, a temperature on the intermediate branch, the melting point and a temperature on the liquid branch, respectively. We see that the intensity of the first peak decreases for the case of Al-Al, Si-Si and Al-O interactions, with increasing temperature. However the position of the first peak, which corresponds to the distance of the first nearest neighbors has almost the same value under temperature effect. This reflects the liquid like behavior, which has a short-range order and hence a solid-like behavior for small values of r.

Figure 4 shows that the second peaks disappear from the distances 5 Å, 5 Å, 3.5 Å and 4 Å for Al-Al, Si-Si, Al-O_H, and O_H-H, respectively, when the solid branch crosses the liquid branch.

For the melting point there is a significant decline in the first peak and an almost flat curve at this temperature, which explains the liquid state of the structure of kaolinite. This phenomenon is repeated and is clearly noticeable for all RDFs.

Finally, the mean-square displacement (MSD) was calculated for Al and O_H under the same temperatures. From the latter quantity (MSD) the diffusion coefficient was deduced according to the following Einstein expression:

$$D = \lim_{t\to\infty} \frac{1}{6t} \left\langle \left| r_i(t) - r_i(0) \right|^2 \right\rangle \quad (7)$$

where $r_i(0)$ and $r_i(t)$ are the initial and final positions of the center of mass of the particle at time t, and $\langle |r_i(t) - r_i(0)|^2 \rangle$ is the MSD averaged over the ensemble.

The diffusion coefficient can be calculated graphically from the slope of MSD vs. time, with an error of 0.001. Table 1 shows the diffusion coefficient for all atoms, Al, Si, O_A, O_Si, O_H, and H. As we may see, the diffusion coefficient is much higher in the liquid branch than in the solid one. In the intermediate branch, a significant increase in the diffusion coefficient as a function of temperature is noticed. The diffusion coefficient of atoms at the melting point is between 2 to 17 times greater than diffusion coefficient at limit of superheating. This confirms the huge thermal agitation of the clay and supports the obtained thermodynamic quantities.

Acknowledgments

A.B. Belonoshko appreciates financial support from the Swedish Research Council (VR).

197

198 **References cited**

199 Ahuja, R., Belonoshko, A.B., and Johansson B. (1998) Melting and liquid structure of
200 aluminium oxide using a molecular-dynamics simulation. Physical Review E, 57, 1673.
201 Allen, M.P. and Tildesley, D.J. (1987, 1989) Computer Simulation of Liquids. Oxford,
202 Clarendon.
203 Belonoshko, A.B. (1994) Molecular dynamics of $MgSiO_3$ perovskite at high pressures:
204 Equation of state, structure, and melting transition. Geochimica et Cosmochimica Acta, 58,
205 4039–4047.
206 Belonoshko, A.B., Skorodumova, N.V., Rosengren, A., and Johansson, B. (2006) Melting and
207 critical superheating. Physical Review B, 73, 012201.
208 Belonoshko, A.B., Davis, S., Skorodumova, N.V., Lundow, P.H., Rosengren, A., and
209 Johansson, B. (2007) Properties of the fcc Lennard-Jones crystal model at the limit of
210 superheating. Physical Review B, 76, 064121.
211 Bish, D.L. (1993) Rietveld refinement of the kaolinite structure at 1.5 K. Clays and Clay
212 Minerals, 41, 738–744.
213 Braterman, P.S., and Cygan, R.T. (2006) Vibrational spectroscopy of brucite: A molecular
214 simulation investigation. American Mineralogist, 91, 1188–1196.
215 Burakovsky, L., Chen S.P., Preston D.L., Belonoshko, A.B., Rosengren, A., Mikhaylushkin,
216 A.S., Simak, S.I., and Moriarty, J.A. (2010) High-pressure—high-temperature polymorphism
217 in Ta: Resolving an ongoing experimental controversy. Physical Review Letters, 104, 255702
218 (4 pages). DOI: 10.1103/PhysRevLett.104.255702

219

220 Chaplot, S.L., Choudhury, N., and Rao, K.R. (1998) Molecular dynamics simulation of phase
221 transitions and melting in $MgSiO_3$ with the perovskite structure. American Mineralogist,
222 83, 937–941.
223 Ciullo, P.A. (1996) Industrial minerals and their uses: a handbook and formulary. Noyes
224 Publications, Westwood, N.J.
225 Cygan, R.T., Liang, J.J and Kalinichev, A.G. (2004) Molecular models of hydroxide,
226 oxyhydroxide, and clay phases and the development of a general force field. Phys. Chem.
227 B, 108, p. 1255–1266.
228 Davis, S.M., Belonoshko, A.B., Johansson B., Skorodumova, N.V., and Van Duin, A.C.T.
229 (2008) High-pressure melting curve of hydrogen. Journal of Chemical Physics, 129,
230 194508.
231 Davis, S.M., Belonoshko, A.B., Johansson B., and Rosengren, A. (2009) An atomistic model
232 for homogeneous melting, KHT Publication Database DiVA.
233 Davis, S.M., Belonoshko, A.B., Rosengren, A., Van Duin, A.C.T., Johansson B. (2010)
234 Molecular dynamics simulation of zirconia melting. Cent. Eur. J. Phys. 8(5), 789–797.
235 Ewald, P.P. (1921) Die Berechnungoptischer und elektrostatischer Gitterpotentiale. Ann.
236 Phys, 64, 253.
237 Frenkel, D. and Smit, B. (1996) Understanding Molecular Simulation. Academic Press, San
238 Diego.
239 Greathouse, J.A., and Cygan R.T. (2005) (2005) Molecular dynamics simulation of uranyl
240 (VI) adsorption equilibria onto an external montmorillonite surface. Phys. Chem., 7, 3580–
241 3586.
242 Hoover, W.G. (1985) Equilibrium phase-space distributions. Phys. ReV.A, 31, 1695.

Kalinichev, A.G., Wang, J., Kirkpatrick, R.J. (2007) Molecular dynamics modeling of the structure, dynamics, and energetics of mineral–water interfaces: application to cement materials. Cem. Concr. Res, 37, 348–350.

Kalra, A., Parks, D.M., and Rutledge, G.C. (2007) Molecular Simulation of Strain Dependence of Vibrational Frequencies for Montmorillonite Clay and Analysis of Strain Transfer in a Polymer-Clay Nanocomposite. Macromolecule, 40, 140–144.

Kirkpatrick, R.J., Kalinichev, A.G., Hou, X., and Struble, L. (2005) Experimental and molecular dynamics modelling studies of interlayer swelling: water incorporation in kanemite and ASR gel. Materials and Structures, 38, 449–458.

Landman, U., Luedtke, W.D., Barnett, R.N., Cleveland, C.L., and Ribarsky, M.W. (1986) Faceting at the silicon (100) crystal-melt interface: Theory and experiment. Physical Review Letters, 56, 155–158.

Larentzos, J.P., Greathouse, J.A and Cygan, R.T. (2007) An ab initio and Classical Molecular dynamics investigation of the structural and vibrational properties of talc and pyrophyllite. Journal of Physical Chemistry C, 111, 12752–12759.

Matsui, M., and Price, G.D. (1991) Simulation of the pre-melting behaviour of MgSiO3 perovskite at high pressures and temperatures. Nature, 351, 735–737.

Mazo, M.A., Manevitch, L.I., Gusarova, E.B., Shamaev, M.Y., Berlin, A.A., Balabaev, N.K., and Rutledge, G.C. (2008a) Molecular dynamics simulation of thermomechanical properties of Montmorillonite crystal. 3. Montmorillonite crystals with PEO oligomer intercalates. Journal of Physical Chemistry B, 112, 3597–3604**.**

Mazo, M.A., Manevitch, L.I., Gusarova, E.B., Shamaev, M.Y., Berlin, A.A., Balabaev, N.K., and Rutledge, G.C. (2008b) Molecular dynamics simulation of thermomechanical properties of Montmorillonite crystal. 1. Isolated clay nanoplate. Journal of Physical Chemistry B, 112, 2964–2969.

Mazo, M.A., Manevitch, L.I., Gusarova, E.B., Shamaev, M.Y., Berlin, A.A., Balabaev, N.K., and Rutledge, G.C. (2008c) Molecular dynamics simulation of thermomechanical properties of Montmorillonite Crystal. II. Hydrated montmorillonite crystal. Journal of Physical Chemistry C, 112 (44), 17056–17062.

Melchionna, S., Ciccotti, G., and Holian, B.L. (1993) Hoover NPT dynamics for systems varying in shape and size. Molec.Phys., 78, 533.

Morris, J.R., Wang, C.Z., Ho, K.M., and Chan, C.T. (1994) Melting line of aluminum from simulations of coexisting phases. Physical Review B, 49, 3109–3115.

Murray, H.H. (2000) Traditional and new applications for kaolin, smectite, and palygorskite: a general overview. Appl. Clay Sci, 17, 207.

——— (2007) Applied clay mineralogy, occurrences, processing and application of kaolins, bentonites, palygorskite-sepiolite, and common clays. Developments in Clay Science, 2.

Smith, W. and Forester, T.J. (1996) The DL_POLY molecular simulation package. Molecular Graphics, 14, 136. http://www.cse.clrc.ac.uk/msi/software/DL_POLY/

Vasconcelos, I.F. and Bunker, B.A. (2007) Molecular Dynamics Modeling of Ion Adsorption to the Basal Surfaces of Kaolinite. Journal of Physical Chemistry C, 11, 6753–6762.

Verlet, L. (1967) Computer “Experiments” on Classical Fluids. I. Thermodynamical Properties of Lennard-Jones Molecules. Physical Review, 159, 98.

Wang, J., Kalinichev, A.G., Kirkpatrick, R.J., and Cygan, R.T. (2005) Structure, energetics, and dynamics of water adsorbed on the muscovite (001) surface: A molecular dynamics simulation. Journal of Physics and Chemistry B, 109, 15893–15905.

Zheng, Y., Zaoui, A., and Shahrour, I. (2010) Evolution of the interlayer space of hydrated montmorillonite as a function of temperature. American Mineralogist, 95, 1493–1499.

——— (2011) A theoretical study of swelling and shrinking of hydrated Wyoming montmorillonite. Applied Clay Science, 51, 177–181.

293

294

295 **Figure Caption**

296

297 **FIGURE 1.** Projection along the **bc**-direction of the unrelaxed structure of a kaolinite sheet
298 formed by $4 \times 2 \times 3$ unit cells (**a**), and after 400 ps equilibration. O atoms are in red, the
299 tetrahedral Si atoms in brown, octahedrally coordinated Al atoms are in gray, and H atoms are
300 white.

301 **FIGURE 2.** Variation of temperature vs. pressure (Z-method) showing the three parts: solid,
302 intermediate, and liquid.

303 **FIGURE 3.** Snapshots of the structure of kaolinite: at two temperatures on the solid branch
304 isochore (**a**), in the intermediate branch (**b**), in the liquid branch and at the lowest temperature
305 (melting point) (**c**), and at a higher temperature of the structure (**d**).

306 **FIGURE 4.** Radial distribution function g(**r**) showing the solid state (repeated peaks) and
307 liquid-like state with flat curve as well the corresponding coordination numbers n(**r**) for
308 various temperatures.

309

Table1: Diffusion coefficient of Al, Si, O and H under various temperatures.

	Diffusion coefficient (10^{-9} m^2/s)					
Temperature/atoms	Al	Si	O_2A	O_2S	O_2H	H_
T= 1688K	0.261	0.002	0.002	0.001	0.013	0.013
T_{LS}=1971K	0.590	0.011	0.025	0.008	0.060	0.063
T= 1911K	0.956	0.040	0.104	0.046	0.226	0.229
T_m=1818K	1.018	0.119	0.254	0.136	0.767	0.767
T= 2261K	2.193	1.035	1.330	1.183	2.560	2.556

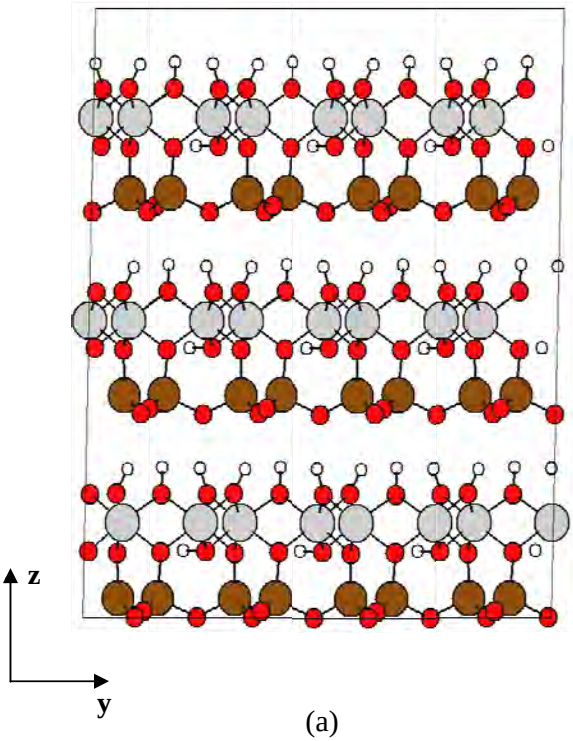

(a)

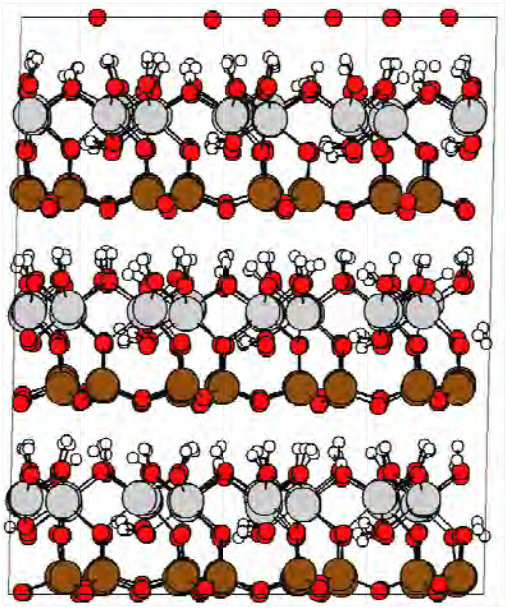

Fig. 1

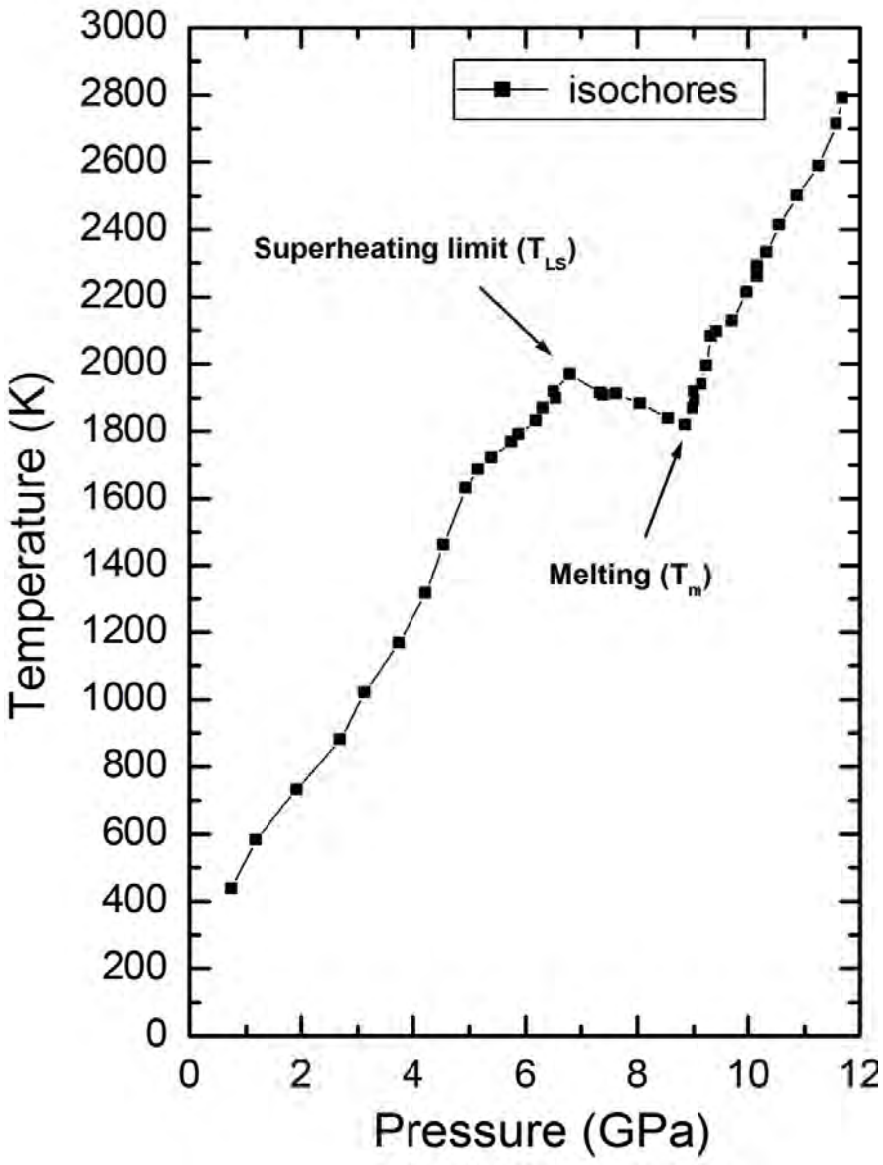
isochores
Superheating limit (T_{LS})
Melting (T_m)
Temperature (K)
Pressure (GPa)
0
200
400
600
800
1000
1200
1400
1600
1800
2000
2200
2400
2600
2800
3000
0
2
4
6
8
10
12

Fig. 2

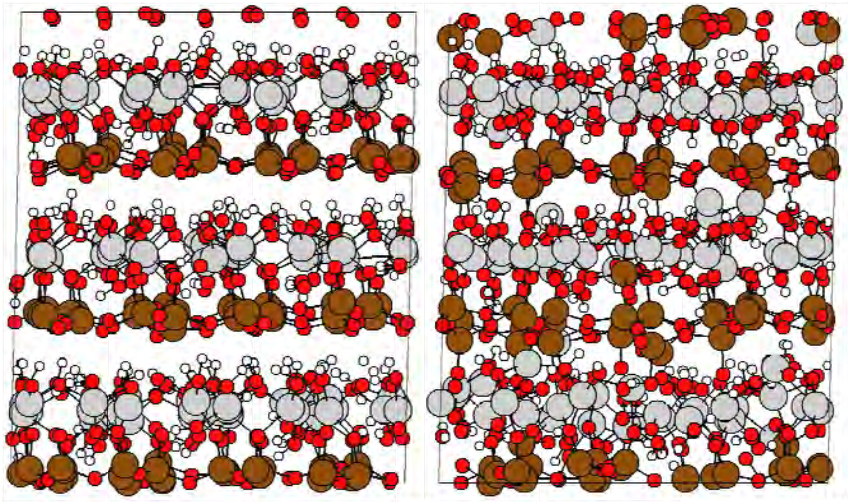

1631K 1971K(a)

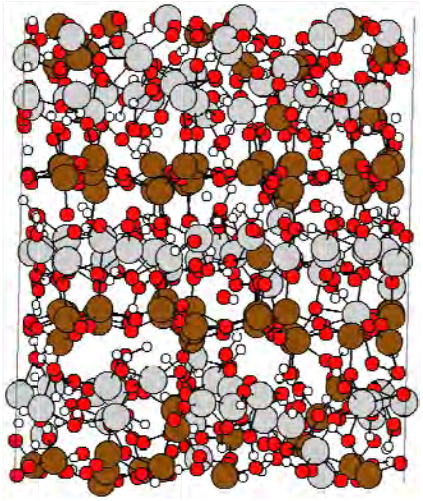

1911K (b)

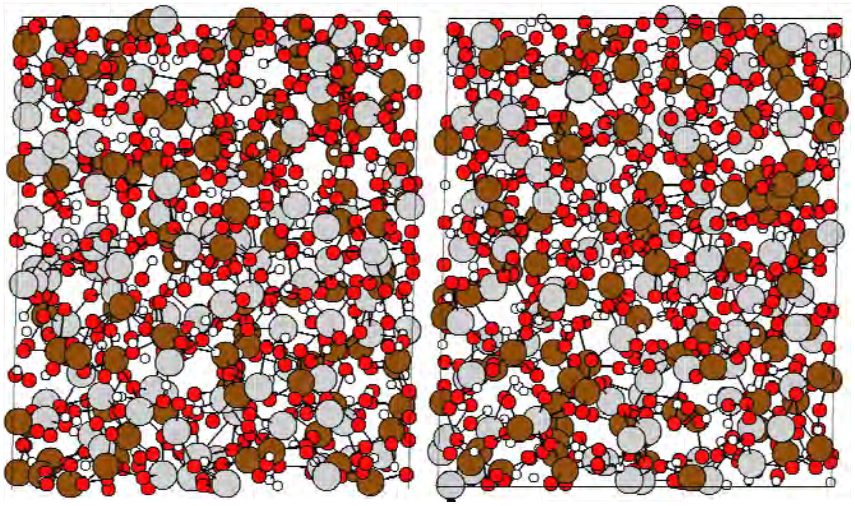

1818K (c) 2261K (d)

Fig. 3

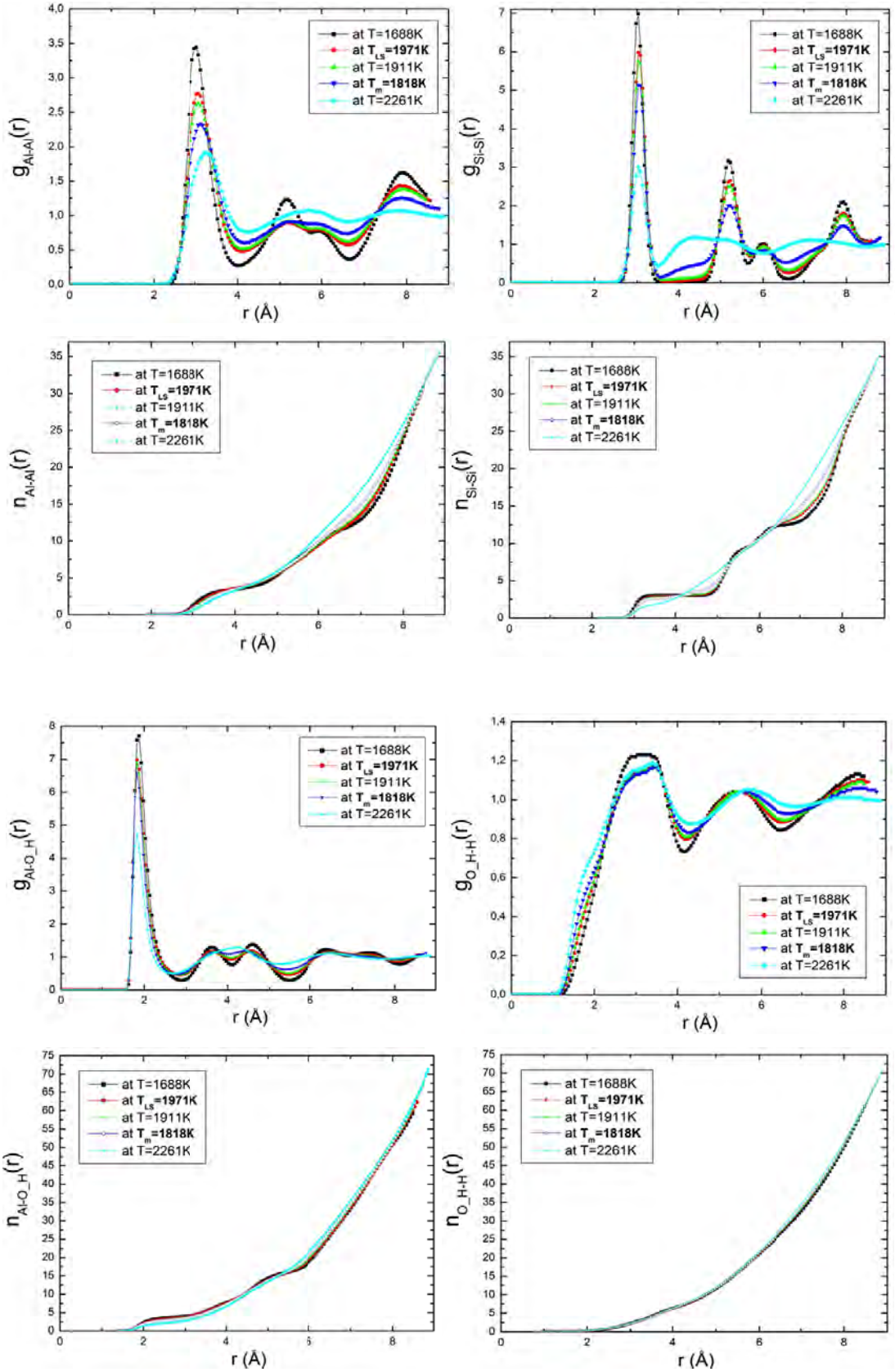
$g_{Al-Al}(r)$
$g_{Si-Si}(r)$
$n_{Al-Al}(r)$
$n_{Si-Si}(r)$
$g_{Al-O\_H}(r)$
$g_{O\_H-H}(r)$
$n_{Al-O\_H}(r)$
$n_{O\_H-H}(r)$
r (Å)
at T=1688K
at T_{LS}=1971K
at T=1911K
at T_m=1818K
at T=2261K

Fig.4